MEDDOCS Open Access Publisher

Annals of Forensic Science and Research

Open Access | Research Article

# FT-IR Spectroscopic Study of Coronary Artery in Cardiovascular Patients and Mathematical Simulation Model of Covid-19 Binding

***Anastassopoulou Jane[1]*; Mylonas Evangelos[2]; Michali Evrydiki[1,3]; Lazopoulos Konstantinos[4]; Kotoulas Christophoros[5]; Theophanides Theophile[1]; Mamarelis Ioannis[6]; Markouizou Athina[7]; Spiliopoulos Konstantinos[2]***

*[1]National Technical University of Athens, Radiation Chemistry & Biospectroscopy, National Technical University of Athens, Greece.*

*[2]Institute of Structural Analysis and Antiseismic Research, National Technical University of Athens, Greece.*

*[3]Consultant in Haematology, Genimatas General Hospital, Mesogeion Ave 154, Athens, Greece.*

*[4]14 Theatrou & Logothetidi, Rafina, 19009, Greece.*

*[5] Cardiothoracic Surgery Department, Metropolitan General Hospital of Athens, Greece.*

*[6]Director of Cardiac Dept. Cardiology Department, 401 General Army Hospital of Athens, Athens, Greece.*

*[7]Department of Radiation Oncology, Metaxa Cancer Hospital, Piraeus, Greece.*

***Corresponding Author(s): Anastassopoulou Jane**

National Technical University of Athens, Radiation Chemistry & Biospectroscopy, Zografou Campus, 15780, Athens, Greece.

Tel: +306973013308; Email: i.anastassopoulou@gmail.com

Received: Sep 26, 2022

Accepted: Oct 27, 2022

Published Online: Oct 31, 2022

Journal: Annals of Forensic Science and Research

Publisher: MedDocs Publishers LLC

Online edition: http://meddocsonline.org/



**Keywords:** Infrared spectroscopy; Covid-19; Amyloids; AGEs; Fractional-order; Λ-fractional derivative.

**Abbreviations:** AGEs: Advanced Glycation End Products; CD: Cardiovascular Diseases; FDE: Full Disc Encryption; FT-IR: Fourier Transform Infrared; FPDEs: Fractional Partial Differential Equations; LADM: Laplace Adomian Decomposition Method; ODE: Ordinary Differential Equations; SIR: Susceptible, Infected, Recovered; Λ-SIR: Lazopoulos Susceptible Infected Recovered.

## Abstract

**Background/Aim**: The characterization of infrared spectroscopic "biomarker bands" induced by diseases can be used to develop mathematical simulation models to approach the mechanism of risk factors in relation to Covid-19 disease in cardiovascular patients, reducing mortality and optimizing hospitalization

**Materials and methods**: For the study, Seventy-two specimens from patients (54-76 years) who underwent coronary endarterectomy during coronary artery bypass grafting were collected. The FT-IR spectra were recorded using a Thermo Scientific Nicolet 6700 instrument. The Λ-SIR fractional derivative for susceptible, infected, and recovered patients and the Caputo fractional derivative have been considered for simulation.

**Results**: FT-IR spectroscopic absorption bands revealed important "biomarker bands" at about 1744 $cm^{-1}$ and 1157 $cm^{-1}$, assigned to aldehyde and advanced glycation end oxidation products, suggesting the oxidative stress involvement on the pathways of inflammatory and stenosis development. The formation of amyloid protein formation in cardiac-diabetic patients and patients suffering from amyloidosis enhances the Covid-19 binding and increase the risk of intubation and mortality. The mathematical simulation Λ- SIR fractional improved thecardiac patients with diabetes type II who are at the highest risk of all patients to COVID-19 attack. This simulation model was found to be in accordance with FT-IR spectroscopic data and clinical aspects.

**Cite this article:** Anastassopoulou J, Mylonas E, Michali E, Lazopoulos K, Kotoulas C, et al. FT-IR Spectroscopic Study of Coronary Artery in Cardiovascular Patients and Mathematical Simulation Model of Covid-19 Binding. Ann Forensic Sci Res. 2022, 1(1): 1006.

**Summary:** FT-IR spectroscopy and Λ-SIR fractional simulation models are important tools to characterize the "biomarker bands" and to discriminate the risk factors of the diseases. Patients suffering from diseases inducedby oxidative stress are at higher risk of hospitalization. At the same risk are people with heart amyloidosis. The mathematical provided that type II diabetic patients with coronary heart disease are at the highest risk susceptible to Covid-19. Next in order are diabetics without coronary heart disease, smokers, and hypertensive people. Comorbidities and personal genetic factors increase risk.

## Introduction

The pandemic Covid-19 respiratory syndrome has infected many people, while epidemiological, clinical and laboratory investigations showed that patients with cardiac comorbid have an increased risk of mortality [1]. Covid-19 belongs to the family of beta-coronavirus phylogeny with a single-stranded positive-sense RNA [1,2]. Electron microscopy revealed that the spike is a clove-shaped trimeric, with three subunits with amino N- and carboxyl C-terminal domains and fusion peptides [2-6]. An envelope-anchored spike protein mediates coronavirus entry into host cells firstly by binding to a host receptor and then by fusing viral and host membranes [4]. The first Covid case in Greece was confirmed on 26th February 2020 [7]. Due to the rapid transmission of COVID-19, the Greek Government in order to control the virus's spread in the population imposed several measures of social distancing. Among the Covid-19 affected patients, a significant proportion of those suffering from cardiovascular diseases recovered slowly or died.

From the time of the discovery of infrared radiation (heat rays)by William Herschel in 1800 astrophysicists applied to study the planetary atmosphere as a chemical system. However, in "live systems" the application of infrared spectroscopy started in late 1940 [8-10]. With the use of the Michelson interferometer (1951) as the infrared spectrometer, the recording of the spectra became more sensitive [11]. For the next decade, instrumentation and computer development demonstrated the feasibility of Fourier Transform Infrared (FT-IR) spectroscopy equipped with crystals that minimize the ratio signal-to-noise. In the last decade, a number of papers have proven that FT-IR spectroscopy benefit when used in pre-diagnosis and diagnosis of diseases [12-19]. FT-IR spectroscopy is a powerful non-invasive physicochemical method and provides the ability to work with small quantities of liquids, tissues, and single cells without any special preparation, as in histopathology. The importance of the method is the rapid spectral scans obtained by co-adding spectra and recording all the components of the sample simultaneously in a very short measurable time [11-17]. The obtained complex spectra, by resolution, provide the ability to identify a few characteristic frequencies of functional groups, such as OH, NH, $PO_2^-$, $COO^-$, $CH_3$, and $CH_2$. Intensity and shape changes, as well as shifts in frequency absorptions, are taken into consideration in order to study the fluctuations induced by the diseases at a molecular level.

Nowadays, scientists use mathematical epidemiology models to describe rapid outbreaks that occur in a short time, while endemic models are used for studying diseases over longer periods, during which there is a renewal of susceptibles because of new births or recoveries from temporary immunity. Famous mathematicians, such as Laplace, Lagrange, Euler, Poincare, and Riemann developed fractional calculus as a better mathematical model for the description of the real-world [20]. The main difference from the conventional analysis is the inherent non-locality of fractional derivatives, important for the description of viscoelasticity. The SIR (Susceptible, Infected, Recovered) epidemic models are used to explain the dynamics of people in a community who need medical attention during an epidemic [21]. The classic SIR model was introduced by Kermack and McKendrick in 1927 to describe the chance of a person spreading the disease and the number of infected or non-infected [21]. The SIR model is commonly used for disease modeling, in particular, for the Covid-19 analysis. In most studies, the authors assume that the recovery rate is constant. The main difference from the conventional analysis is the inherent non-locality of fractional derivatives that is important for the description of viscoelasticity [23], which is an important parameter for cardiovascular diseases [22], a parameter important for cardiovascular diseases. In order to overlap the problem, Lazopoulos induced in the SIR model the Λ-fractional derivative [21,22].The Λ-fractional derivative satisfies the prerequisites of differential topology, necessary for variation problems in fields such as the non-linear problem of the pandemic of Covid-19 [22,23]. Using the new computational method Laplace Adomian Decomposition Method(LADM) is possible to find the solution to the Λ -SIR fractional model. LADM is an effective and straightforward technique for nonlinear Fractional Partial Differential Equations (FPDEs). Furthermore, LADM requires fewer parameters and is without any discretization and linearization [23,24]. Other advantages include the wide applicability to several types of problems and scientific fields, and the development of a reliable, numerical solution[23,24].

In the present paper, FT-IR spectroscopy was used to analyze the most important products produced during the development of cardiovascular diseases. Furthermore, the mathematical simulation models and correlation of the Λ-fractional derivative were used to approach the mechanism of Covid-19 action in patients with cardiovascular diseases in our country [7].

## Materials and methods

For FT-IR spectroscopic study seventy-two specimens from patients (54-76 years) who underwent coronary endarterectomy during coronary artery bypass grafting were collected.

### Statement of ethics

The samples were obtained according to the principles of the Helsinki declaration and the Greek law of ethics for ex vivo clinical research.

### Mathematical simulation model

To perform the mathematical simulation model 1848 patients were taken, among which 771 were during the first Covid-19 lockdown, dated from 10th March 2020 to 10th May 2020, and 1077 were in the normal routine period a year before the pandemic, which is considered a normal period. The patients were recorded according to their cardiovascular risk factors [7,25]. For the simulations, the Λ-fractional derivative andthe Caputo fractional derivative have been considered. The ode45 MATLAB routine for the system ODE in the Λ space and the FDE2 MATLAB routine for the FDE system in the Caputo case was applied.

### FT-IR spectroscopy

FT-IR spectra were recorded by using a Thermo Scientific Nicolet 6700 spectrometer. Each spectrum has consisted of 120

co-added spectra with a resolution of 4 $cm^{-1}$. The samples after surgery were fixed in formalin and after 5 days were washed with distilled water and dehydrated under vacuum at room temperature.

## Results & discussion

### FT-IR spectral interpretation

The selection of representative FT-IR spectra of coronary arteries among the patients was based on assignment factors [7]. Figure 1 illustrates the spectra of coronary arteries received from healthy (a), diabetic type II patients (b), and patients suffering from amyloidosis (c).

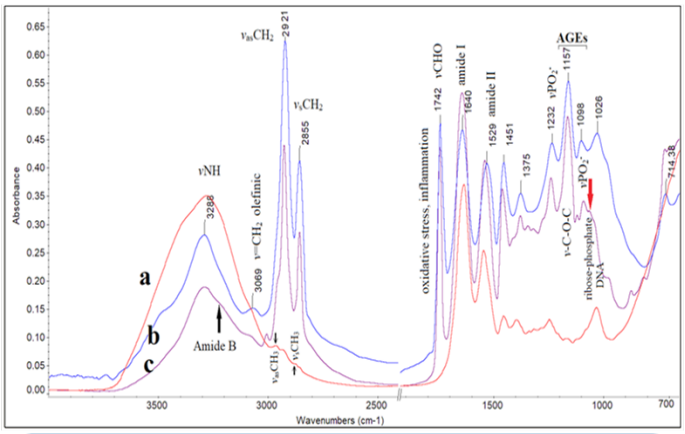


**Figure 1:** Representative FT-IR spectra of coronary arteries. **(a)** Healthy, **(b)** from a patient with amyloidosis, and **(c)** diabetic type II patient, in the spectral regions: 4000-2500 $cm^{-1}$ and 1800-700 $cm^{-1}$. On the spectra are noticed the characterizations of the most important bands.

It is known that amyloidosis causes the deposition of misfolded fibrillar proteins in the extracellular space[26]. A comparison of the spectra b and c shows similarities in almost all frequencies. The intensity decrease of the stretching absorption bands and assignments of *ν*NH groups, resulting mostly from the proteins, indicates protein damage. The intensity reduction of *ν*NHis more obvious in the spectra of the patient with amyloidosis. The appearance in the spectrum c, of the patient diagnosed with cardiac amyloidosis, of a broad band at about 3200-3100 $cm^{-1}$ leads to the result that the proteins changed the conformational structure from the native form of α-helix to Amide B conformation, as it was expected. We have seen that this band is a "marker band" of amyloid protein formation [13-17]. The high-intensity increase of the asymmetric $\nu_{as}CH_2$ and symmetric $\nu_{as}CH_2$stretching vibration bands of methylene groups at 2921 $cm^{-1}$ and 2855 $cm^{-1}$, respectively. The absorption bands of asymmetric $\nu_{as}CH_3$ and symmetric $\nu_{as}CH_3$ stretching vibration bands of methyl groups are reduced or almost disappeared. These bands are caused by lipids and phospholipids, predominant membrane lipids. On the contrary, in spectra of healthy persons, the stretching vibrational bands of methyl and methylene groups appear as very weak shoulders. This indicated an increase in the lipophilic environment of both coronary arteries of the non-healthy patients.

The very intense absorption band at 1742 $cm^{-1}$, assigned to the stretching of the aldehyde *ν*CHO band, is the "marker band" of oxidative stress and inflammation [12,13,27]. It was noticed that the intensity of this absorption band increases with the progression of the disease and is related to the involvement of oxidative stress in the pathways of the disease. This suggestion is in agreement with the appearance of the band at about 3069 $cm^{-1}$, assigned to the stretching vibration band of the olefinic bond *ν*=$CH_2$ with olefinic character as radical termination products, revealing the dysregulation of lipid metabolism. The intensity of this band is related to the LDL of the patients [28]. Furthermore, in the spectra of diabetic type II patients, the spectra showed a distinguishable band at about 1729 $cm^{-1}$, assigned to cardiolipin [29].

As is shown from the spectra b and c of the patients the frequencies of the amide I and amide II bands of CONH atoms of the peptide bond shift lower from 1650 $cm^{-1}$ and 1545 $cm^{-1}$ to 1640 $cm^{-1}$ and 1529 $cm^{-1}$, respectively. These shifts illustrate that the native conformation of α-helix changed and motifs of the β-sheet structure have been formed [11-16,30]. The amide bands are very sensitive to diseases and can be used as diagnostic bands. The developed lipophilic environment was confirmed by the intensity increase of the asymmetric and symmetric vibrations of methylene groups allowing the proteins susceptible to auto assemblies. This transition yields protein aggregates and fibrils to systemic amyloidosis, which was observed in many pathological conditions, such as Alzheimer's, neurodegenerative, cancer, and diabetes type II [31]. The findings are in accordance with the clinical history of both patients and the FT-IR collected spectra originating from the diabetic type II (spectra b) and amyloidosis (spectra c) patients are almost similar. However, in patients with amyloidosis, coronary angiography displays the absence of obstructive atherosclerotic disease and normal to close-to-normal coronary arteries [32].

The next fingerprint spectral region between 1240-1000 $cm^{-1}$comparison of the spectra originated from the patients **(Figure 1b,c)** with that originated from healthy persons shows intensity and shape changes. The stretching vibration absorption band at 1232 $cm^{-1}$, assigned to $\nu PO_2^-$, of phospholipids and DNA is pronounced in the spectra of patients, revealing the progress of non-reversible phosphorylation. Proteins, because of their high abundance in the cells are the main substrate for non-enzymatic lipid peroxidation phosphorylation reactions **(Figure 2)** and have been observed in diabetic patients [33,34].These modifications induce changes in the physicochemical and biological properties of cell membranes and are accumulated upon diabetes and amyloidosis. Another important observation was the band intensity increase at about 1157 $cm^{-1}$, assigned to the stretching *ν*C-O of C-O-C vibrational mode where the oxygen atom is linked to two carbon atoms of the sugar moiety of glycosaminoglycans together with the exocyclic C-O-C intermolecular group [14]. In the spectra of the patient with amyloidosis (Figure 1c) the frequency shows a small but significant shift to higher wavenumbers at 1161 $cm^{-1}$. We have seen that in the case of cancer this band appears to have even higher frequencies up to 1170 $cm^{-1}$ [14-17]. These bands confirm the progression of glycosylation and the production of advanced glycation end products (AGEs) [14-17].Glycoxidation of proteins causing fibril and AGEs products in non-enzymatic metabolism (Millard reactions) is associated with ROS (Reactive Oxygen Species) generation and hyperglycemia elevates the glycation mixtures and influences the fibril formation. The formation of aldehyde derivatives, as is noticed from the band at 1742 $cm^{-1}$ enhances the formation of AGEs [35]. By using inhibitors, the researchers have shown ascorbyl free radicals elevation of AGEs level [36,37].

Studies have shown that Covid-19 leads to cellular damage activating the local immune system and releasing pro-inflammatory [38]. Our FT-IR spectroscopic analysis showed as a result of the diseases, an increase in the lipophilic cell environment,

inflammation, protein folding dysregulation, phosphorylation, and elevated glycation products (AGEs) depending on the disease's progression. Covid-19 causes similar products and is suggested that these products are rearrangement in the lipophilic environment of the host cells and their transformation for viral replication. By glycosylation, the NH terminal and OH groups increase, and the number of targeting sites for SARS-CoV-2 spike attack increases. **Figure 2** illustrates schematically the produced pathways caused by the oxidative stress upon the progression of the disease.

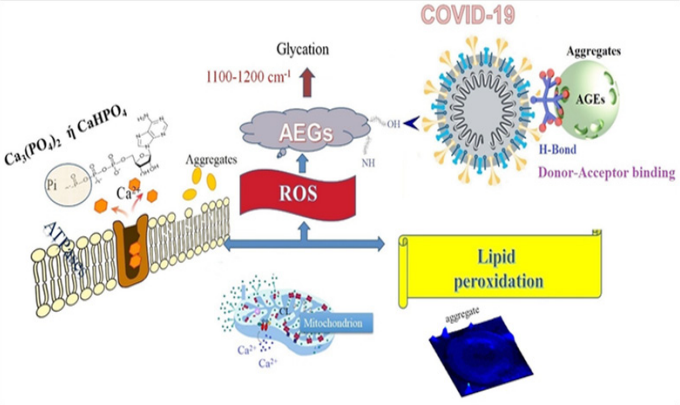


**Figure 2:** Schematic presentation of peroxidation products of coronary artery of diabetic type II patient and interaction pattern between oxidation products caused by the disease and a Covid-19 spike binding. The formation of aggregates was detected using a hypermicroscope Olympus-cyto-Vita.

The proposed mechanism is a result of FT-IR spectroscopic data which revealed the formation of a high lipophilic environment and amyloid proteins while promoting the severe progression of the disease in patients. This structure of the host is quasi-similar to that of the SARS-CoV-2 hydrophobic packing environment and thus a patient's ideal for target cell attachment.

### Λ-fractional derivative Covid-19 simulation model

The novel Λ-SIR computation model is a powerful tool to evaluate the infected and recovered heterogeneous hosts of SARS-CoV-2,involving healthy and those with comorbid conditions. Despite the personal clinical history of the patients, the recovery rate and morbidity depend on the time of recovering process such as intensive care, including the number of hospital beds and treatment [22,23]. For the study, the investigated population is divided into three compartments which are the susceptible (S), the infected (I), and the recovered (R) groups **(Figure 3)**.

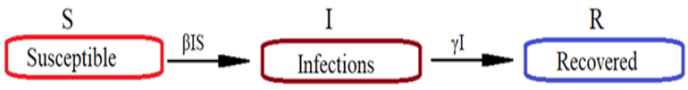


**Figure 3:** Schematic illustration of compartments of Covid-19 spreading pathways of Susceptible, Infected, Recovered (SIR) patients.

This model is represented by a system of ordinary differential equations (ODE) which describe the changes across the population. The following equations (1)-(3) are used:

$$\frac{dS(t)}{dt} = -\beta S(t)I(t) \quad (1)$$

$$\frac{dI(t)}{dt} = -\beta S(t)I(t)\text{-}\gamma I(t) \quad (2)$$

$$\frac{dR(t)}{dt} = -\gamma I(t) \quad (3)$$

Where S(t), I(t)>0, R(t) ≥ 0, and S+I+R=N, and N is the total population, β represents the infection parameter where a patient is transferred from the susceptible group to the infected group while γ represents the parameter where a patient is transferred from the infected to the recovered group. From these parameters, the basic reproduction ratio is given:

$$R_0 = \frac{\beta N}{\gamma} \quad (4)$$

is used to find the expected number of new infections in a single population. Generally, when $R_0 > 1$, the infection will spread in a population, typically, meaning that an epidemic could hardly be controlled.By using the equations (1)-(3)the Λ-fractional derivative is appliedas follows:

$${}_0^{\Lambda}D_t^k = -\beta S(t)I(t) \quad (5)$$

$${}_0^{\Lambda}D_t^k I(t) = \beta S(t)I(t)\text{-}\delta I(t) \quad (6)$$

$${}_0^{\Lambda}D_t^k = \delta I(t) \quad (7)$$

The non-linear part*S(t)I(t)* may be decomposed by:

$$S(t)I(t) = \sum_i^{\infty} X_i(t) \quad (8)$$

Where

$$X_i = \frac{1}{i!}\frac{d^i}{d\lambda^i}[\sum_{j=0}^{i}\lambda^j S_j(t)\sum_{j=0}^{i}\lambda^j I_j(t)] \quad (9)$$

and *i*=1…n

For the numerical applications, is considered β=0.5,δ=0.3, and t=0 as starting pointsjustbefore the spread of COVID-19. At the same time t=0 the groups are considered, as $S_0$the susceptible population (S(t),t=0), $I_0$ the infected (I(t),t=0), and $R_0$ the initialrecovering population (R(t),t=0) and N the total population consistsof the sum, where: $S_0$=900, $R_0$=10, $I_0$=50, and N=960.

Laplace transform equations (10)-(13) are used to calculate the rate of the susceptible patients for each category:

$$L(S_0(t)) = \frac{s(0)}{s} \quad (10)$$

$$L(S_1(t)) = \frac{\beta}{s}L(X_0(t)) \quad (11)$$

$$L(S_2(t)) = \frac{\beta}{s}L(X_i(t)) \quad (12)$$

$$L(S_{i+1}(t)) = -\frac{\beta}{s}L(X_i t) \quad (13)$$

Figure 4 illustrates the diagrams of the rate susceptibility of patients' subcategories. Curve **a** corresponds to diabetic type II cardiac patients, **b** and **c** correspond to non-cardiac patients who suffer from diabetes type II and hypertensive patients without any cardiac problem, respectively.

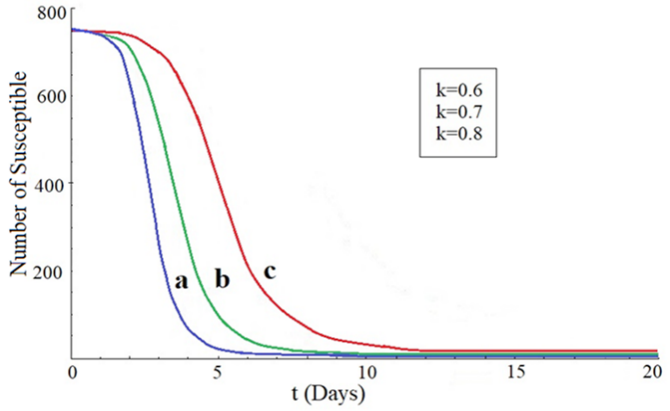


**Figure 4:** Relation between susceptible subcategories of patients by the time model. Curve **a** corresponds to diabetic type II cardiac patients, **b** and **c** correspond to diabetic type II and hypertensive patients without coexistent cardiovascular disease, respectively.

As it is shown from the curves diabetic II with CD patients is more susceptible compared to the other categories. This observation is in accordance with literature data, that was noticed around the world from the beginning of the pandemic. For calculation of the infected people, of each category, the equation (14) and the general form (15), where i=1,2,3…n, were used:

$$L(I_0(t)) = \frac{I(0)}{s} \quad (14)$$

$$L(I_{i+1}(t)) = \frac{\beta}{s} L(X_i(t)) - \frac{\delta}{s} L(I_i(t)) \quad (15)$$

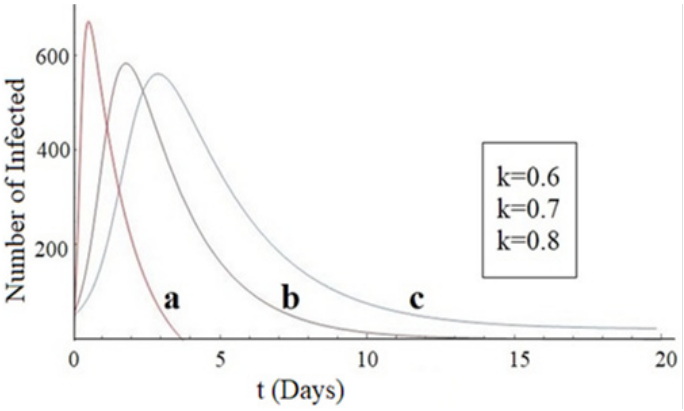


**Figure 5:** Model of the relation between infected patients of the subcategories of by the time. Curve correspond: **a;** to diabetic type II cardiac patients, **b;** non-cardiac patients who suffer from diabetes type II and **c;** hypertensive patients without any cardiac problem with risk factors k=0.8, 0,7, 0,6, respectively.

The received curves are presented in **Figure 5**. It is also shown that diabetic type II patients are at the highest risk for infection. A comparison of the curves received from diabetic type II patients made clear that cardiac patients are at an increased risk of morbidity and mortality. A comparison between the three categories shows that hypertensive patients show a better prognosis against Covid-19. This model predicts again that cardiac comorbidities increase the risk of infection.

To estimate the performed simulation model for Covid-19 risks of recovered patients we included patients with intubation. To investigate the dynamic of the model the exertion was based on the next 20 days' forecast of the ultimate situation. For calculations of the recovered subgroups the equations (16) and (17), with i=1,2,3…n, were used:

$$L(R_0(t)) = \frac{R(0)}{s} \quad (16)$$

$$L(R_{i+1}(t)) = \frac{\delta}{s} L(I_{i+n} i(t)) \quad (17)$$

The results are displayed in Figure 6. From these results is concluded that diabetic type II cardiac patients are at higher risk of recovering, while incubated patients show the best prognosis for recovering. The model predicted very well the expected results [7,27]. Moreover, is suggested that a well-organized healthcare system minimizes the risk of mortality [26].

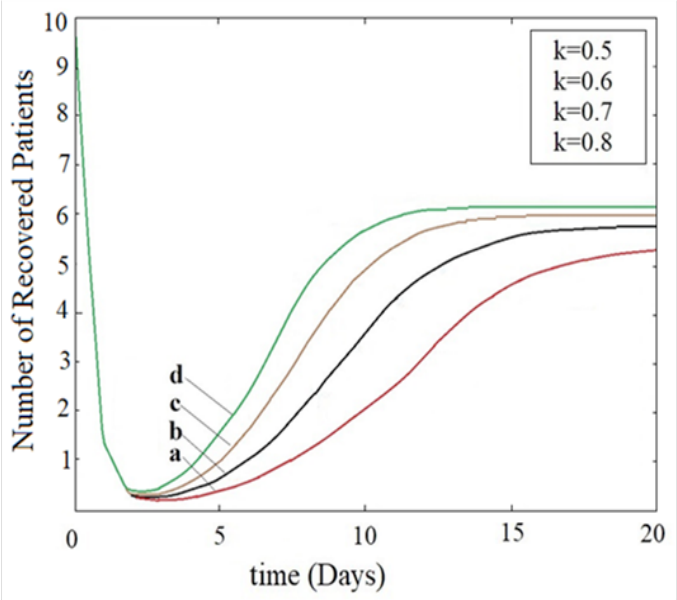


**Figure 6:** Λ-SIR simulation model of the relation between recovered patients with time. Curves correspond: a; diabetic type II with cardiovascular disease, b; non-cardiac patients who suffer from diabetes type II, c; hypertensive patients without coexistent cardiovascular disease, and d; patients with intubation, where k=0.8, 0,7, 0,6 and 05, respectively.

The simulation models highlight that cardiovascular patients with diabetes type II comorbidities are at the highest probability of risk for infection with Covid-19 or death. The next category of non-cardiac diabetic type patients compared with those with CD is at less risk of accessibility to the virus. Hypertension, one common risk associated with age, showed a lower probability of Covid-19 infection among the three categories. In general, the model could discriminate the risk factors induced by disease. Moreover, the model could be applied to more complex patients with comorbidities.The simulation models are in accordance with the results of FT-IR spectroscopic data, where was observed that coronary arteries damage depends on many factors, such as diabetes, hyperuricemia, environment, and parametersthat induce oxidative stress [18,30,40].

## Conclusions

FT-IR spectroscopic "marker bands" at 1744 $cm^{-1}$ and 1165 $cm^{-1}$ provide important information regarding the effect of oxidative stress on aldehyde and AGEs production, respectively. These products are correlated with inflammation, amyloid protein deposits, and glycosylation. The intensity increase of stretching vibrations of methylene bands at *v*2921 and 2855 $cm^{-1}$ indicates the increase of membrane lipophilicity and aggregates formation. Accumulation of AGEs and amyloids increases the targeting sites of Covid-19 spike glycoproteins binding the cell membranes. Both FT-IR spectra and Λ-SIR fractional deriva-

tive epidemic mathematical modeling are important tools to discriminate and predict the risk probability of the disease progression and patients' morbidity and mortality. In general, the SIR-Λ-fractional derivative model showed that diabetic type II patients are at the highest risk of Covid-19, while patients with heart amyloidosis show similar behavior. Smokers are more susceptible than hypertensive patients. In addition, the risk probability increases in patients with co-existent comorbidities and personal genetic problems, obesity, and diet.

## References


1. Guzik TJ, Mohiddin SA, Dimarco A, Patel V, Savvatis K, et al. COVID-19 and cardiovascular system: implications for risk assessments, diagnosis and treatment options. Cardiovasc Res. 2020; 116: 1666-1687.
2. Kirchdoerfer RN, Cottrell CA, Wang N, Pallesen J, Yassine HM, et al. Pre-fusion structure of a human coronavirus spike protein. Nature. 2016; 531: 118-121.
3. Lecis R, Mucedda M, Pidinchedda, E, Molecular identification of Betacoronavirusin bats from Sardinia (Italy): first detection and phylogeny. Virus Genes. 2019; 55: 60-67.
4. Li F. Structure, Function, and Evolution of Coronavirus Spike Proteins. Annu Rev Virol. 2016; 3: 237-261.
5. Walls AC, Tortorici MA, Bosch BJ, Frenz B, Rottier PJ, et al. Cryoelectron microscopy structure of a coronavirus spike glycoprotein trimer. Nature. 2016; 531: 114-117.
6. Kirchdoerfer RN, Cottrell CA, Wang N, Pallesen J, Yassine HM, et al. Pre-fusion structure of a human coronavirus spike protein. Nature. 2016; 531: 118-121.
7. Kanakakis I, Stafylas P, Tsigas G, Nikas D, Synetos A, et al. Epidemiology, reperfusion management, and outcomes of patients with myocardial infarction in Greece: The ILIAKTIS study. HJC 2022; 67: 1e8.
8. Blout ER, Mellors RC. Infrared spectra of tissues. Science. 1949; 110: 137-138.
9. Fraser RDB. Infra-red microspectrometry with a 0.8 N.A. reflecting microscope. Discuss Faraday Soc.1950; 9; 378-383.
10. Woernley DL. Infrared absorption curves for normal and neoplastic tissues and related biological substances. Cancer Res. 1952; 12; 515-523.
11. Theophanides T. Infrared Spectroscopy-Life and Biomedical Science, InTech Open. 2012.
12. Theophanides T. Infrared Spectroscopy-Anharmonicity of Biomolecules, Crosslinking of Biopolymers, Food Quality and Medical Applications. InTechOpen. 2015.
13. Anastassopoulou J, Mamarelis I, Theophanides T. Study of the development of carotid artery atherosclerosis upon oxidative stress using infrared spectroscopy and scanning electron microscopy. OBM Geriatrics. 2021; 5.
14. Mavrogenis A, Malesiou E, Tanis O, Mitsiokapa E, Tsatsaragkou E, et al. The influence of sepsis on the molecular structure of bones: A Fourier Transform Infrared spectroscopy study. Journal of Long-Term Effects of Medical Implants. 32: 57-63.
15. Markouizou A, Anastassopoulou J, Kolovou P, Theophanides T, Tsekeris P. Fourier Transform Infrared spectroscopy in the study of discrimination of lobular breast cancers. Cancer Diagnosis &Prognosis (CDP). 2022.
16. Anastassopoulou J, Kyriakidou M, Malesiou E, Rallis M, Theophanides T. Infraredand Raman spectroscopic studies of skin molecular disorders and cancer. In Vivo. 2019; 33: 567-572.
17. Anastassopoulou J, Kyriakidou M, Mamareli V, Tanis O, Rallis M. The influence of UV irradiation on diabetic mice skin. A vibrational FT-IR and Raman spectroscopic study. Chromatogr Spectrosc Tech. 2019; 02: 21-27.
18. Mamarelis I, Koutoulakis E, Kotoulas C, Dritsa V, Mamareli V, et al. Amyloid like formation and aortic valve calcification promoted by oxidative stress. Hellenic J Atherosclerosis. 2016; 7: 84-96.
19. Maiti KS, Roy S, Lampe R, Apolonski A. Detection of Disease-Specific Volatile Organic Compounds Using Infrared Spectroscopy. Eng Proc. 2021; 8:15.
20. Lovergne L, Ghosh D, Schuck R, Polyzos AA, Chen AD, et al. An infrared spectra biomarker accurately predicts neurodegenerative diseases class in the absence of overt symptoms. Scientific Reports 2021; 11:15598.
21. Kermack WO, McKendrick AG. Contributions to the mathematical theory of epidemics-I. Bull Math Biol. 1991; 53: 33-55.
22. Lazopoulos KA. On Λ-fractional differential equations. Foundations. 2022; 2: 726-745.
23. Lazopoulos AK, Karaoulanis D. On -Fractional Viscoelastic Models. Axioms. 2021; 10: 22.
24. Lazopoulos AK. Nonlocal continuum mechanics and fractional calculus. Mech Res Commun. 2006; 33: 753-757.
25. Mohammed OH, Salim HA. Computational methods based Laplace decomposition for solving nonlinear system of fractional order differential equations. Alex Eng J. 2018; 57: 3549-3557.
26. Jafari H, Khalique CM, Nazari M: Application of the Laplace decomposition method for solving linear and nonlinear fractional diffusion-wave equations. Appl Math Lett. 2011; 24: 1799-1805.
27. Papafaklis MI, Katsouras CS, Tsigkas G, Toutouzas K, et al. "Missing" acute coronary syndrome hospitalizations during Covid-19 era in Greece: Medical care avoidance comined with a tru reduction in incidence? Clin Cardiol. 2020; 43: 1142-1149.
28. Martinez-Naharro A, Hawkins PN, Fontana M. Cardiac amyloidosis. Clin Med (Lond). 2018; 18: s30-s35.
29. Halliwell B, Gutteridge MC. Free radicals in biology and medicine, 3rd Edition, New York, Oxford, University Press, 2000.
30. Anastassopoulou J, MamarelisI, Tsiligiris B, et al. The role of free radicals in the development of carotid plaque. A spectroscopic study. In vivo. 2008; 24: 883-888.
31. Kotoulas C, Mamarelis I, Koutoulakis E, KyriakidouM, Mamareli V, et al. The influence of diabetes on atherosclerosis and amyloid fibril formation of coronary arteries. A FT-IR spectroscopic study, Hell J Atheroscler. 2017; 8: 15-29.
32. Fabian H, Nauman D. Protein folding and misfolding. Shining light by infrared spectroscopy. Heidelberg, Dordrecht, London, New York, Springer. 2012.
33. Chiti F, Dobson CM. Protein misfolding, functional amyloid, and human disease. Annu Rev Biochem. 2006; 75: 333-366.
34. Papageorgiou C, Tsagalou W, Baraboutis I, Tampakis K, Kastritis E, et al. Cardiac amyloidosis presenting with coronary artery embolization. Rev Cardiovasc Med. 2021; 22: 883-889.
35. Yu H, Liu Y, He T, Zhang Y, He J, et al. Platelet biomarkers identifying mild cognitive impairment in type 2 diabetes patients. Aging Cell. 2021; 20: e13469.
36. Matveyenka M, Rizevsky S, Kourouski D. Unsaturation in the fatty acids of phospholipids drastically alters the structure and tox-

icity of insulin aggregates grown in their presence. J PhysChem Lett. 2022; 13: 4563-4569.

37. Sadowska-Bartosz I, Galiniak S, Bartosz G. Kinetics of glycoxidation of bovine serum albumin by methylglyoxal and glyoxal and its prevention by various compounds. Molecules. 2014; 19: 4880-4896.

38. Sadowska-Bartosz I, Stefaniuk I, Galiniak S, Bartosz G. Glycation of bovine serum albumin by ascorbate in vitro: Possible contribution of the ascorbyl radical? Redox Biol. 2015; 6: 93-99.

39. Yan SD, Schmidt AM, Anderson GM, Zhang J, Brett J, et al. Enhanced cellular oxidant stress by the interaction of advanced glycation end products with their receptors/binding proteins. J Biol Chem. 1994; 269: 9889-9897.

40. Mamareli V, Tanis O, Anastassopoulou J, Kyriakidou M, Mamareli CH, et al. The role of oxidative stress on molybdenum enzymes and ischemic reperfusion injury in hyperuricaemic patients. An infrared spectroscopic study, Eur J Mol & Clin Med. 2019; 6: 20-25.